The EMBO Journal Vol.19 No.5 pp.892–901, 2000

Properties of lipid microdomains in a muscle cell membrane visualized by single molecule microscopy

Gerhard J.Schütz, Gerald Kada, Vassili Ph.Pastushenko and Hansgeorg Schindler[1]

Institute for Biophysics, University of Linz, A-4040 Linz, Austria

[1]Corresponding author,
e-mail: h.schindler@jk.uni-linz.ac.at

The lateral motion of single fluorescence labeled lipid molecules was imaged in native cell membranes on a millisecond time scale and with positional accuracy of ~50 nm, using 'single dye tracing'. This first application of single molecule microscopy to living cells rendered possible the direct observation of lipid-specific membrane domains. These domains were sensed by a lipid probe with saturated acyl chains as small areas in a liquid-ordered phase: the probe showed confined but fast diffusion, with high partitioning (~100-fold) and long residence time (~13 s). The analogous probe with mono-unsaturated chains diffused predominantly unconfined within the membrane. With ~15 saturated probes per domain, the locations, sizes, shapes and motions of individual domains became clearly visible. Domains had a size of 0.7 μm (0.2–2 μm), covering ~13% of total membrane area. Both the liquid-ordered phase characteristics and the sizes of domains match properties of membrane fractions described as detergent-resistant membranes (DRMs), strongly suggesting that the domains seen are the *in vivo* correlate of DRMs and thus may be identified as lipid rafts.

Keywords: fluorescence imaging/human coronary artery smooth muscle cell/lipid rafts/liquid-ordered lipid phase/single molecule diffusion

Introduction

The lateral organization of the plasma membrane of cells has found a revisited interpretation since the postulation of lipid rafts as structural and functional units for membrane-targeted signaling (Simons and Ikonen, 1997). One support for the raft concept came from the biochemical evidence that certain lipids are not extractable from lysates of cells by non-ionic detergents (Brown and Rose, 1992). Detergent-resistant membranes (DRMs) are membrane fractions rich in glycosphingolipids, cholesterol and glycosylphosphatidylinositol (GPI)-anchored proteins (Sargiacomo *et al*., 1993; Melkonian *et al*., 1995; Anderson, 1998). These properties of DRMs indicate that they may originate from lipid microdomains in the plasma membrane with the need for further physical and functional definition of the *in vivo* correlate of DRMs. It has been suggested that caveolae, morphologically well established invaginations of the plasma membrane (Chang *et al*., 1994; Parton, 1996; Thyberg *et al*., 1997; Anderson, 1998), represent a subclass within the operationally defined detergent-resistant fractions (Schnitzer *et al*., 1995; Harder and Simons, 1997; Brown and London, 1998). They are functional units for folate uptake and cholesterol regulation (Anderson *et al*., 1992; Fielding and Fielding, 1995). The size of these caveolae (~50 nm) is, however, smaller than the sizes of DRMs in electron micrographs (Brown and Rose, 1992; Schnitzer *et al*., 1995). Further support for the existence of rafts came from recent microscopy experiments (reviewed by Jacobson and Dietrich, 1999).

While lipid rafts are known to exist, they have not yet been clearly physically described in terms of size, shape and dynamics, of affinities of membrane components for rafts and their dynamic regulation, and of their relationship to the actin-based cytoskeleton. This is approached here by applying novel fluorescence microscopy, which attains the sensitivity and speed for repeated imaging of single molecules in their motional path (single dye tracing, SDT; Schmidt *et al*., 1996). So far, research at the single fluorophore level using fluorescence labeled biomolecules has focused on mechanistic studies (for a review, see Weiss, 1999), ranging from studying motor proteins (Funatsu *et al*., 1995; Sase *et al*., 1995; Ishijima *et al*., 1998) to enzymatic reactions (Lu *et al*., 1998), or on protein mapping on erythrocytes (Enderle *et al*., 1997).

The present report is the pilot application of single fluorescent molecule microscopy to a living cell. In previous studies using lipid membranes, the potentials of SDT have been demonstrated for analyzing diffusion, co-localization and stoichiometries of single fluorescence labeled molecules (for a review, see Schmidt *et al*., 1999). We now show that SDT enables us to image single lipid probe molecules *in vivo* and to follow their motion on a millisecond time scale with sub-wavelength lateral positioning within ~50 nm. This is used to search for lipid microdomains or rafts in the plasma membrane of human coronary artery smooth muscle (HASM) cells, as areas of confinement and enrichment of a particular probe molecule. Obvious choices for a suitable probe are constituent molecules of DRMs or rafts. Based on findings that lipids and lipidated components in DRMs or rafts have consistently saturated acyl chains (Schroeder *et al*., 1994; Brown and London, 1998), we chose a saturated lipid probe molecule [DMPE (1,2-dimyristoyl-*sn*-glycero-3-phosphoethanolamine)-Cy5] for this investigation, and a mono-unsaturated lipid probe [DOPE (1,2-dioleoyl-*sn*-glycero-3-phosphoethanolamine)-Cy5] for comparison. Images of DMPE-Cy5 in HASM cell membranes provided clear evidence for the existence of lipid microdomains with direct visualization of domain properties. This, and the complementary evidence of no significant preference of DOPE-Cy5 for the domains, strongly suggests that the domains seen are the *in vivo* correlate of DRMs.

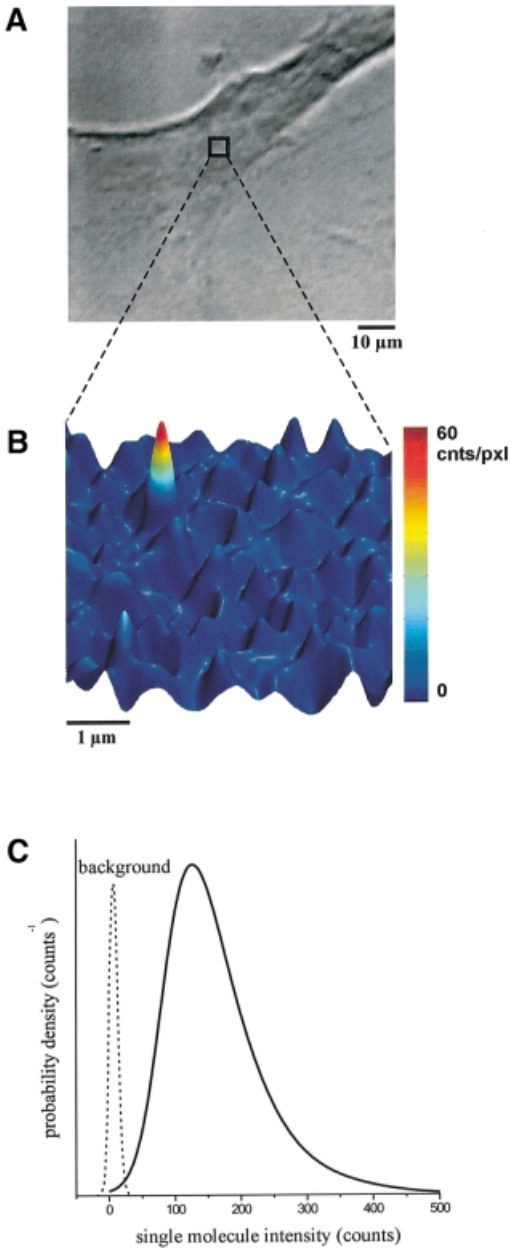

Fig. 1. Single lipid imaging in a cell membrane. (**A**) White light image of an HASM cell pre-treated with DOPE-Cy5 as probe lipid at a magnification of 40×. The square at the center of the cell indicates the area selected for fluorescence imaging. (**B**) The fluorescence image of this area was taken at 100× magnification, yielding a clearly resolved fluorescent peak of a single DOPE-Cy5 molecule. (**C**) Probability density of the single molecule fluorescence intensity taken from 933 observations of 291 molecules of DOPE-Cy5. The mean value of $<F> = 161 \pm 3$ counts agrees perfectly with the value for the single molecule intensity measured in artificial lipid membranes. The low background signal (dotted line, ×10) allows for single molecule detection with a high signal-to-noise ratio of $<S/N> = 23$.

Results

Imaging of single lipid probes

Figure 1A shows a light microscope image of a HASM cell chosen for studying single lipid diffusion in a plasma membrane. Fluorescence labeled lipids (DOPE-Cy5 and/or DMPE-Cy5) were inserted via lipid exchange between lipid vesicles and the plasma membrane of the HASM cell. For fluorescence imaging of the lipids, the focal plane of the excitation light with ~1.6 µm focal depth was adjusted to a sufficiently flat area of the top membrane, of normally 10 × 10 µm size (5 × 5 µm in Figure 1A). The fluorescence image (Figure 1B) shows a clearly resolved peak with a signal-to-background noise ratio of 15 at an illumination time of 5 ms.

In order to confirm that this peak originates from a single lipid probe molecule, we compared the average intensity of many observed peaks for both lipid probes with the predicted intensity known from studying Cy5-labeled lipids in model membranes. The fluorescence intensity for 5 ms illumination of 933 peaks observed in HASM cell membranes gave the distribution shown in Figure 1C. The mean fluorescence intensity is $<F> = 161 \pm 3$ counts, which is in perfect agreement with the single molecule signal of DMPE-Cy5 found for a lipid bilayer environment permitting safe determination of the unitary intensity for reference (Trabesinger, 1997).

The background signal, included in Figure 1C, has a standard deviation of seven counts, which is only 2–3 counts larger than the noise generated during the read-out process of the camera. This shows that the contribution from the background fluorescence of the cell is sufficiently low for clear single dye tracing. The resulting average signal-to-noise ratio $<S/N>$ for detecting single lipid probes in HASM cell membranes is $<S/N> = 161/7 = 23$. This value allows for the determination of the lateral position of the molecules to within 54 nm (Bobroff, 1986; Schütz *et al*., 1997), which represents the resolution of lipid probe motion in trajectories of peak positions for repeated illumination (for 5 ms each throughout this study).

Tracing the insertion of a single lipid probe and its lateral motion

The transfer process of a single lipid probe from a lipid vesicle into the plasma membrane was observed directly (Figure 2). Figure 2A shows the three main stages of this process. On the top, a vesicle prepared to contain 4 ± 2 DMPE-Cy5 lipid probe molecules (see Materials and methods) just touches the focal plane, as judged from the low intensity peak seen. After 70 ms, the vesicle has attached to the membrane and becomes visible as a high intensity signal of 745 counts, which indicates the presence of five lipid probes in the vesicle. The next observation, at 105 ms, shows the vesicle peak with reduced intensity (621 counts), where adjacent to it a second peak of 120 counts appeared, indicating that one of the five lipid probes has been inserted into the plasma membrane during the vesicle–membrane encounter time of <105 ms. Clear evidence for this was obtained from following the motions of both the vesicle and the single probe, by repeated imaging every 35 ms. Figure 2B shows the trajectories of the vesicle and of the probe molecule (limited to 14 images for technical reasons, cf. Materials and methods). The size of the data points represents the accuracy of positioning of the probe molecule and the vesicle within each image. Both trajectories start from the same position and then separate (positions 3 and 4 correspond to the second and third image in Figure 2A). It can clearly be seen that the vesicle resides at the membrane, indicating attractive vesicle–membrane interactions. Analysis of its trajectory by a routine algorithm (Schmidt *et al*., 1995)

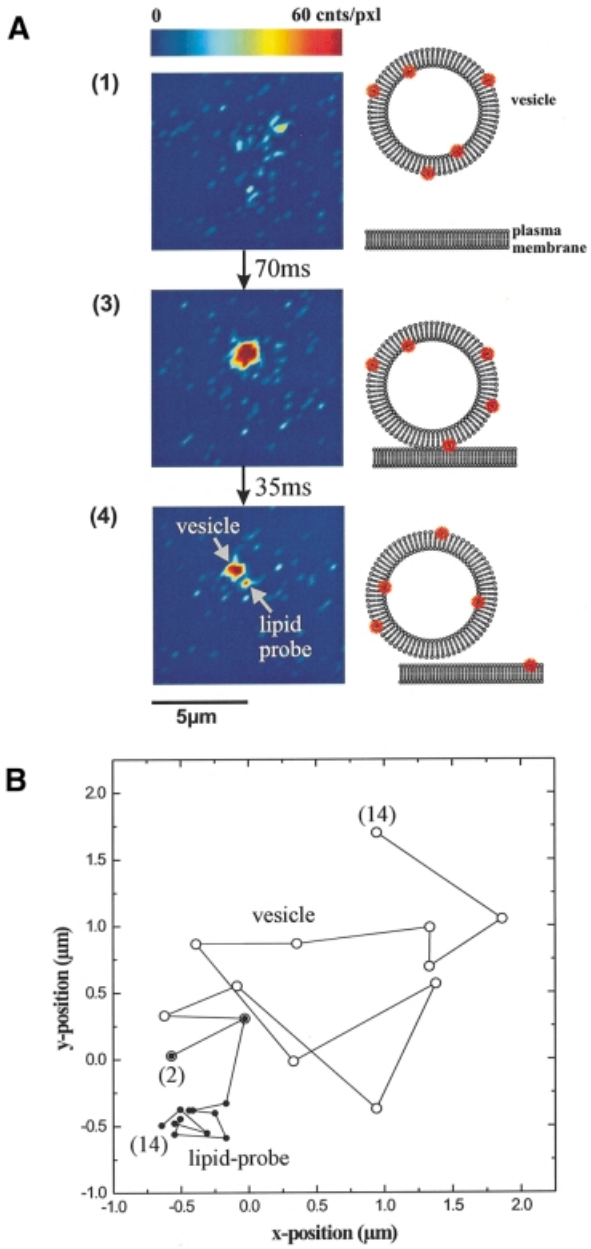

Fig. 2. Insertion of a single lipid probe molecule into the plasma membrane of an HASM cell. (**A**) The fluorescence image shows an area of 10 × 10 µm on the top surface of the cell. A very small number of vesicles containing DMPE-Cy5 as probe lipid were applied. In the first image, only a small fluorescence signal can be observed, corresponding to a vesicle entering the focal plane of the objective. After 70 ms, the vesicle, which can be observed as a bright spot, has attached to the membrane. After another 35 ms, a second, much smaller fluorescence signal appears, which represents the unitary intensity of a single DMPE-Cy5 molecule. (**B**) The trajectories of the lipid molecule (●) and the vesicle (○) have been constructed from a sequence of 14 consecutive images with a delay of 35 ms. Before lipid insertion, positions (2) and (3), vesicle and lipid probe are still co-localized. After insertion, positions (4)–(14), the two trajectories reveal a much higher mobility of the vesicle compared with the lipid molecule. The images corresponding to positions (3) and (4) are shown in (A).

yields a two-dimensional Brownian motion of the vesicle with a diffusion constant of $D = 3.0 \pm 0.1$ µm^2/s. Apparently, the attractive interactions also lead to a reduction of the surface mobility of the vesicle since for

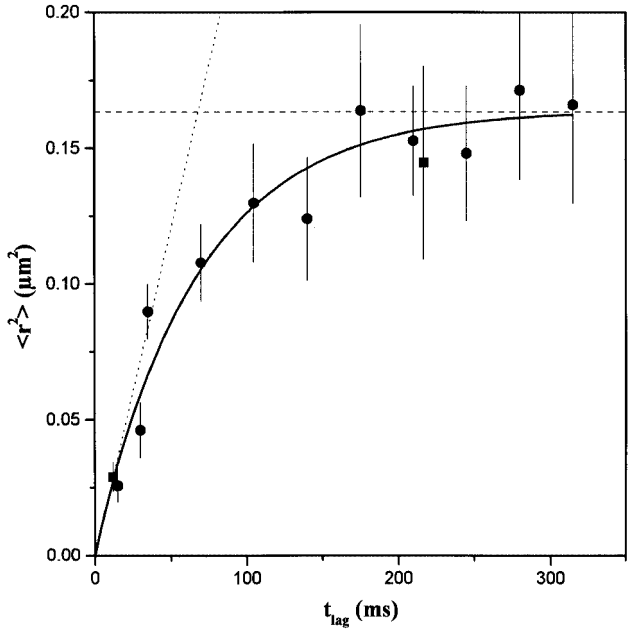

Fig. 3. Mobility of single DMPE-Cy5 lipid molecules. The mean square displacement, $<r^2>$, as a function of the time lag shows saturation for $t_{lag} > 100$ ms. A total of 145 trajectories of different single molecules have been analyzed (●), yielding a diffusion constant $D = 0.6 \pm 0.04$ µm^2/s for lipid probe motion within the domain (dotted line) and a domain size of 700 ± 20 nm (dashed line), when the data are fitted to the model of restricted diffusion (solid line). Mean square displacements of 43 molecules for alternating short (12 ms) and long (212 ms) time lags are included (■).

its free diffusion in the aqueous space a value of ~25 µm^2/s is predicted (Huang and Mason, 1978).

The trajectory of the lipid probe (DMPE-Cy5) reveals two features of interest. The overall motion is far from being random, but appears to be restricted to an area of ~500 nm size. This confinement of the probe to an area, however, does not impede fast mobility within this area since the displacements between consecutive positions in the trajectory of Figure 2B were characterized by a relatively high diffusion constant of $D = 0.9 \pm 0.2$ µm^2/s.

A saturated lipid probe (DMPE-Cy5) senses fluid microdomains

Inspection of a large number of trajectories of single DMPE-Cy5 molecules showed that fast but restricted diffusion is a general characteristic of this lipid probe in HASM cell membranes. For this, the cell membranes were loaded with the lipid probe to a concentration of ~1 probe/50 µm^2 (cf. Materials and methods), and areas 10 µm in size were imaged repeatedly. In Figure 3, the data from 145 trajectories are summarized by plotting the mean square displacements, $<r^2>$, for each time lag in the trajectories. $<r^2>$ values do not increase linearly with the time lag as would be predicted for free Brownian diffusion. Instead, displacements show a maximum value, as expected for restricted diffusion. The data are well fitted by assuming free diffusion within a square area of size L surrounded by an impermeable barrier (Kusumi *et al.*, 1993). Best fit (solid line) yielded a mean domain size of $L = 700 \pm 20$ nm and a diffusion constant of $D = 0.60 \pm 0.04$ µm^2/s for lipid probe motion within the domain. In this model, D represents the initial slope of

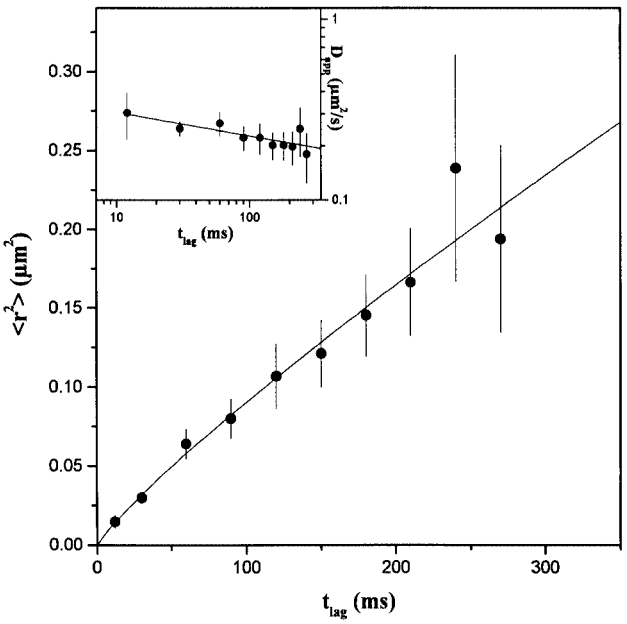

Fig. 4. Mobility of single DOPE-Cy5 lipid molecules. The mean square displacement, $<r^2>$, as a function of the time lag is shown for the data from 291 single molecule trajectories. In the insert, a double-logarithmic plot of the apparent diffusion constant $D_{app} = \langle r^2 \rangle / 4t_{lag}$ is shown as a function of the time lag. It is fitted to the model of anomalous subdiffusion $\langle r^2 \rangle \propto t^{\,a}_{lag}$ (full line in both graphs) yielding an exponent $\alpha = 0.87 \pm 0.02$.

the curve (dotted line) and L the maximum value of $<r^2>$ (dashed line). For comparison, we determined L and D from maximum likelihood analysis of the mean displacements, resulting in $L = 620 \pm 30$ nm and $D = 0.94 \pm 0.13$ µm²/s. Finally, in a particular set of experiments (square data points in Figure 3), single lipid trajectories were recorded for alternating short (12 ms) and long (212 ms) delay times, thus focusing on fast short-range diffusion and on restricted long-range motion, for the same molecules. The match of these data with the curve of best fit further strengthens the conclusion that this lipid probe occurs (with at least high preference) in confinement areas of ~620–700 nm in size within which it moves with a relatively high diffusion constant of 0.6–0.9 µm²/s.

An unsaturated lipid probe (DOPE-Cy5) predominantly diffuses within the membrane

When applying the same experimental protocol to a lipid with mono-unsaturated acyl chains (DOPE-Cy5), the single lipid trajectories revealed a qualitatively different mode of motion compared with DMPE-Cy5, which has saturated acyl chains. Figure 4 shows the data from 291 trajectories of single DOPE-Cy5 lipids. Displacements increase monotonously with increasing delay time. The increase is not strictly linear as would be expected for Brownian diffusion. In a logarithmic plot (see the insert of Figure 4), the relationship is linear, according to $\langle r^2 \rangle \propto t^{\,a}_{lag}$ with $\alpha = 0.87 \pm 0.02$. This increase without any saturation within the accessible range of lag times clearly shows that at least most of the DOPE-Cy5 probes are freely diffusing within the cell membrane.

Properties of microdomains: size, shape, mobility and occurrence

The evidence so far for the existence of lipid microdomains was obtained from the behavior of single molecules in time. This analysis, based on sequential observation in time, was complemented by the alternative approach of studying the behavior of small ensembles of lipid probes at the same time. For this, the concentration of inserted lipid probe DMPE-Cy5 was increased ~100 times compared with the single probe studies, resulting in average densities of a few probes per square micrometer. Images for 5 ms illumination time now showed not single molecules but single domains, as seen in Figure 5A. This directly confirms that the probe molecules are highly localized in domains that contain, on average, 15 lipid probes. The density of the probe had been set to this value since it allowed both for best contrast and for sufficient smooth images of the domains (sufficient overlap of the images of the individual probes distributed over the domain area). The apparent variability of domain shape made an estimate of the mean domain size difficult. Therefore, each domain was characterized by a value for the area, A, enclosed by a contour line taken at half of the peak intensity of the respective domain. The domain size, d, was estimated according to $d = 2\sqrt{A/\pi} - d_0$, where $d_0 = 270$ nm corrects for the widening of the domain size by diffraction (see the black lines in Figure 5). The resulting sizes of 22 domains found on one cell are plotted in Figure 5B. The mean domain size is 710 nm, in perfect agreement with the value obtained from single probe trajectories. However, the histogram shows that the majority of values distribute about a smaller 'typical size' of 500 nm, with two sizes at much larger values. Such large deviations from the 'typical size' were often seen in images of domains and may well represent associations of smaller units (see the substructure of the domains in Figures 5A and 6). Moreover, domains appeared non-uniform not only with respect to size and shape, but also with respect to mobility. Evidence for this was obtained from trajectories of single domain motions, again by repeated imaging with 5 ms illuminations.

The results from repeated imaging were quite surprising to us. The majority of domains stayed in place even on a minute time scale. For some domains, slow fluctuations within ~200 nm about the holding position could be resolved. This is shown for three domains in Figure 5A. Such fluctuations of domains from the same image occurred in uncorrelated directions, which excludes membrane drift as their origin. For some domains, trajectories revealed uni-directional movements. A particular example is shown in Figure 5A. A large elongated domain, which gives the appearance of a linear association of smaller domains, slowly rotates in one direction while held fixed at one end. Another example is a linear uni-directional movement of domain 3 in Figure 6 (cf. legend). None of the various domains analyzed by trajectories showed free diffusion; they either remained in place or moved uni-directionally.

It should be noted that these results apply to the middle (sufficiently flat) part of the top membrane of the HASM cells. Here, the domains were not distributed randomly; their density and organization varied considerably from

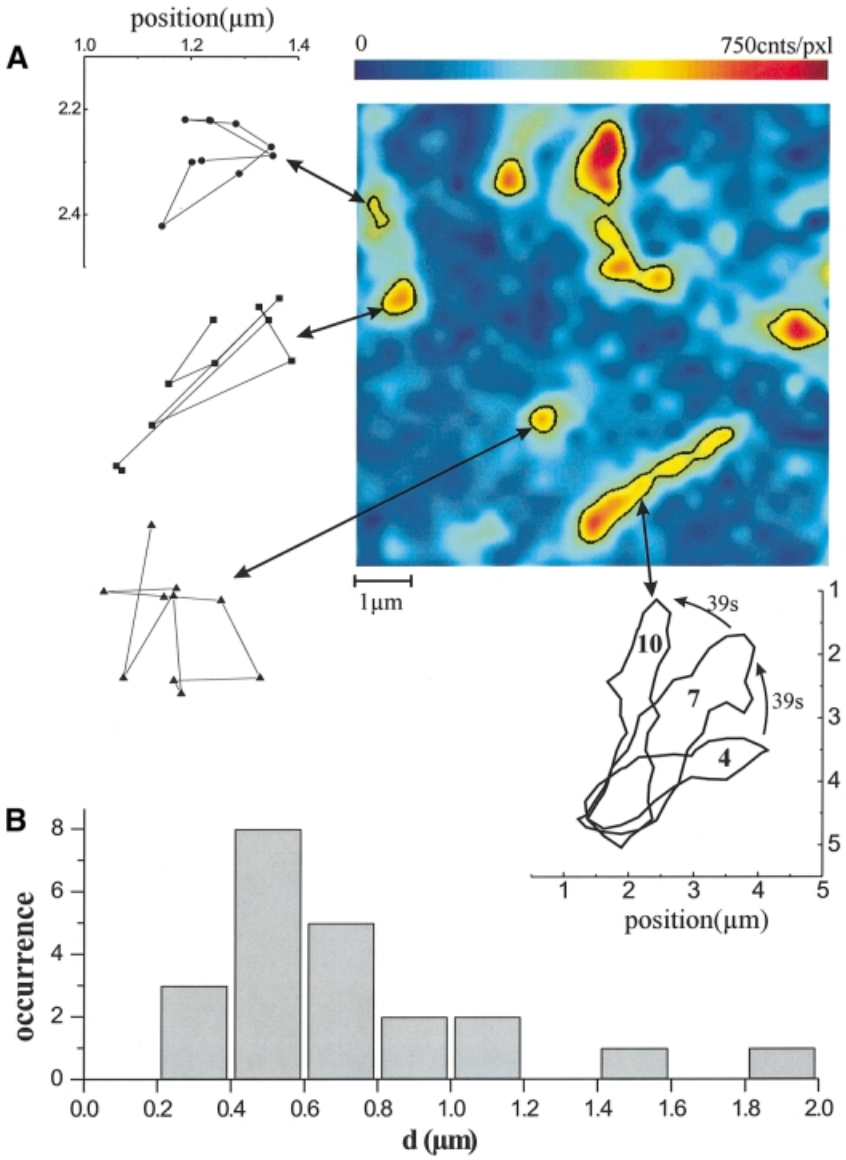

Fig. 5. Single domain imaging. (**A**) The image was taken at the top surface of an HASM cell after insertion of a high concentration of DMPE-Cy5 as probe lipid. Single domains can clearly be observed as bright fluorescent areas, containing on average ~15 lipid probe molecules. For illustration, each domain was highlighted by a black contour line drawn at the half-maximum value of the respective fluorescence intensity. The mobility of individual domains was analyzed by determining the position of the domain center on consecutive images, as shown for three domains (left). The delay between two observations was set to 13 s. Uni-directional rotation has been observed for the domain at the bottom of the image, as exemplified for images 4, 7 and 10 by domain contours. (**B**) Histogram of the estimated domain diameters (see the text).

area to area. The only consistent feature found was the fraction of area covered by domains, which was ~13%.

Partition coefficient and exchange rate of DMPE-Cy5 between domains and bulk membrane

The analysis of single DMPE-Cy5 trajectories indicated a high partition coefficient of this probe into domains, which, however, provided no basis for quantification. The same applied to single domain images, where the number of lipids within domains could be counted, but the number of probes outside domains could not be counted to sufficient accuracy due to higher background noise (cf. Materials and methods). Quantification was possible, however, by determining the initial rate of fluorescence recovery after photobleaching (FRAP) the domains. One example is shown in Figure 6. The fluorescence of the five domains seen (Figure 6A) was bleached (Figure 6B) and the onset of fluorescence recovery was sampled every 13 s (Figure 6D). We limited the experiment to eight repeats in order to keep the cumulative bleaching during recovery low. Two data sets (open and filled circles) refer to domains 1 and 2 (cf. Figure 6B), which stayed in place within 200 nm (see image after 104 s in Figure 6C). The trajectory of domain 3 showed uni-directional movement, as indicated, and considerable shape change during this movement, while domain 4, which initially appeared to have sub-domains (Figure 6A), stretched during this time into a linear set of smaller domains. Domain 5 showed little recovery, while a new domain appeared at the bottom of Figure 6C. The recovery of fluorescence within the total area (see triangles in Figure 6D) had virtually the same characteristics as the recovery of domains 1 and 2,

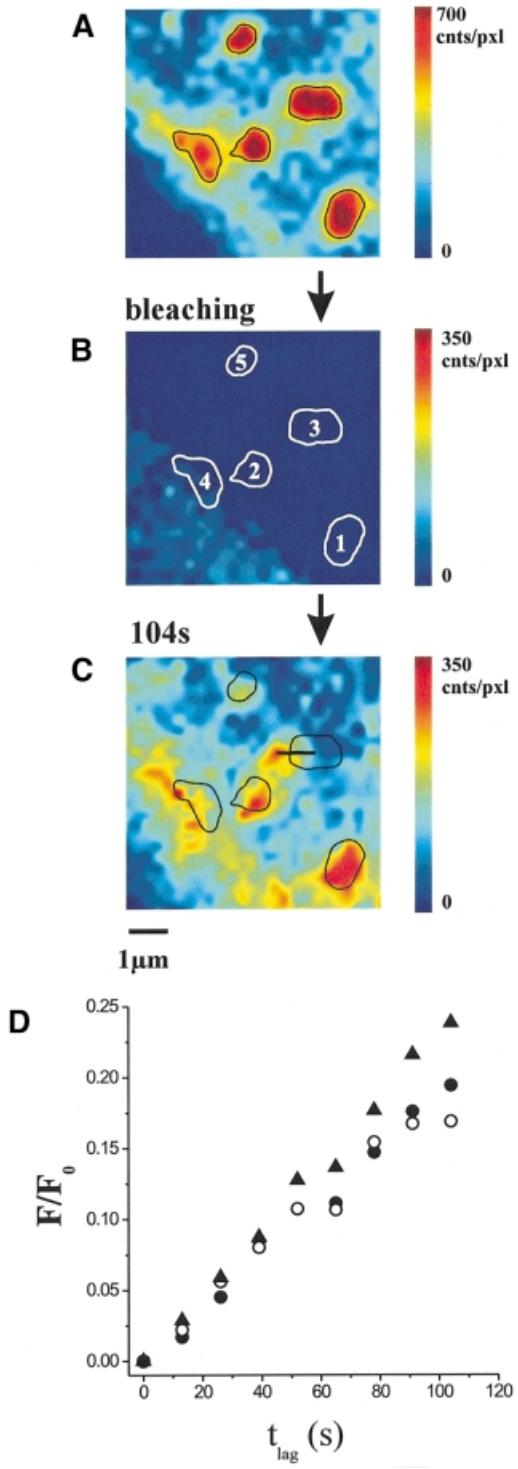

Fig. 6. Single domain FRAP. (**A**) FRAP was studied for the domains seen. (**B**) An area of 8 µm was bleached, which contained the image area. Recovery of the fluorescence due to lipid probe diffusion into the bleached area was monitored every 13 s. The image (**C**) shows fluorescence recovery after 104 s. (**D**) The fluorescence recovery of domain 1 (●) and 2 (○) was analyzed by determining the intensity every 13 s by integrating over the domain area (black contour). For comparison, the fluorescence recovery within the whole image area is included (▲). All values (F) were normalized to the respective initial value (F_0) obtained from (A). In (C), the trajectory of the center of domain 3 is included, showing uni-directional motion.

indicating that the initial recovery flux of lipid probes from outside into domains within this area is fairly unaffected by changes of domain organization and number within the time of analysis.

The normalized rate of recovery, $r = \mathrm{d}[F(t)/F_0]/\mathrm{d}t$ in Figure 6 initially is constant at ~0.1/50 s. This rate r depends on the diffusion constant, D, and on the concentration of the probe outside domains, C_{out}, according to $r = \mathrm{d}[F(t)/F_0]/\mathrm{d}t = \mathrm{d}[N(t)/N_0]/\mathrm{d}t = \frac{1}{N_0} N_0 2\pi C_{out} D/\ln(b/L)$ (Szabo *et al.*, 1980). N_0 and $N(t)$ are the number of probes in the image area before bleaching and during recovery, respectively. Geometry enters by $\ln(b/L)$, with b the size of the area effectively bleached (b ~8 µm) and L the domain size. This formula is the two-dimensional equivalent of the formula for diffusion-controlled reaction in three dimensions (see, for example, Atkins, 1978). It has previously been shown to apply to association processes in membranes (Hinterdorfer *et al.*, 1997). Setting $N_0 = C_{dom}A$, where C_{dom} is the probe concentration in domains and A the area covered by domains, yields $r = 2\pi DC_{out}/[\ln(b/L)C_{dom}A]$. The partition coefficient $p = C_{dom}/C_{out}$ is then obtained from $p = 2\pi D/[rA\ln(b/L)]$. This yields an estimate for the partition coefficient of DMPE-Cy5 between domains and bulk membrane of p ~100. This value, together with the area fraction of 13% covered by domains, indicates that only 7% of the lipid probes are freely diffusing in the bulk membrane outside domains. Using the above formula but inserting for A the mean domain area (0.4 µm^2) and for b the mean distance between domains (1.7 µm), the rate r now gives an estimate for the exchange rate k of the probe between domains and bulk membrane, yielding k ~1/13 s. This rate indicates that the probe diffuses, on average, ~80 times across the domain before it desorbs into the bulk membrane. This justifies the assumption of an impermeable barrier for the estimation of the domain size from the data of single probe trajectories in Figure 3. It has to be noted that we used here a saturated lipid probe with a relatively short chain length compared with naturally occurring lipids and with the unsaturated probe, since for this short chain the exchange rate was just measurable within the time limit set by domain mobility and life time.

Simultaneous imaging of the saturated and the unsaturated lipid probes

In analogy to the studies of DMPE-Cy5, we complemented the DOPE-Cy5 data in Figure 4 by imaging this probe also at high concentration, under the same conditions as used for the saturated lipid probe for imaging domains. At this ensemble level of the unsaturated probe, we addressed two questions: (i) is the probe distributed randomly over the membrane plane, as predicted from the single probe diffusion data (Figure 4); and (ii) to what extent does the unsaturated probe partition into the domains where the saturated probe highly enriches? This required independent knowledge of the areas covered by domains. For this, we simultaneously imaged in the same area the unsaturated probe DOPE-Cy5 and the saturated lipid probe with, however, a different fluorescence label [DMPE-tetramethylrhodamine (TMR)], which fluoresces in the green. Figure 7A shows an image of DMPE-TMR with one

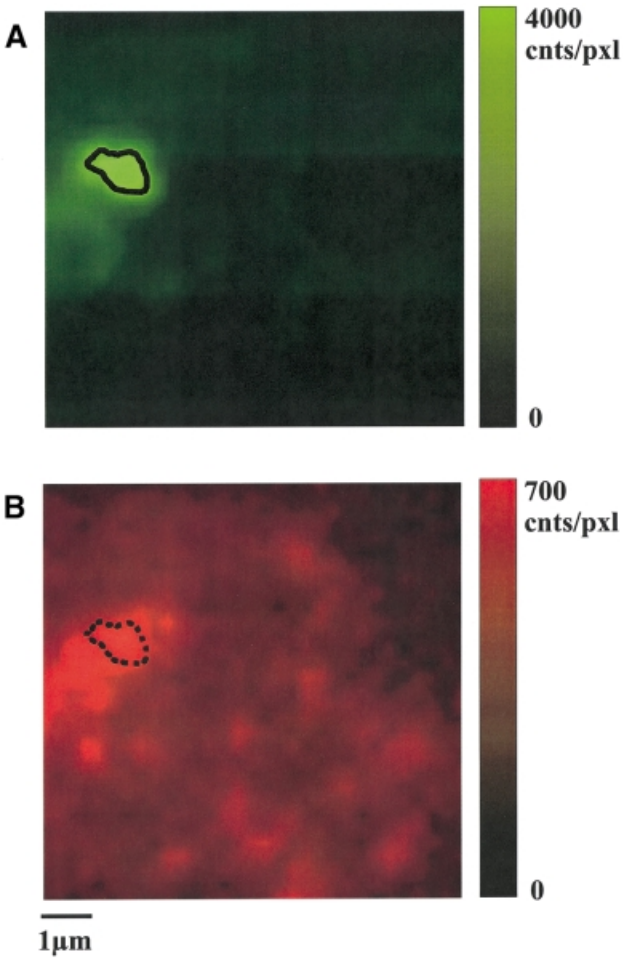

Fig. 7. Two-color imaging of DMPE-TMR (**A**) and DOPE-Cy5 (**B**). Each image represents the average of five consecutive images in a sequence of 10 images (t_{ill} = 5 ms) for alternating excitation wavelengths of 528 nm (selective excitation of DMPE-TMR) and 633 nm (selective excitation of DOPE-Cy5). This allows simultaneous imaging of DMPE-TMR in lipid domains (A), and of the distribution of DOPE-Cy5 (B). Only a slight increase in fluorescence intensity at the respective location of the domain (indicated by the dashed line) can be found [note the different scales in (A) and (B)]. Intensity variations observable in (B) are expected for this low concentration regime due to statistical fluctuations of the local number of DOPE-Cy5 molecules. Analysis of the number of lipid probes per diffraction-limited area yields a Poisson distribution with a variance of 2.1 probes/4 pixels, which is in good agreement with the mean density of 9 probes/μm^2, providing further evidence for a random distribution of the probe.

large and clearly visible domain. In contrast, DOPE-Cy5 is spread over the entire area (Figure 7B). The variations in intensity reflect changes of the probe area density about a mean of ~10 probes/μm^2. When sampling equal sub-areas of the image (cf. legend), the fluorescence signals were well represented by a Poisson distribution, with a variance equal to the mean, confirming that the unsaturated probe was distributed randomly in the membrane plane. It is noteworthy that complementary fluctuations of probe density in time were seen in repeated images with characteristic times consistent with single probe diffusion (Figure 4). During unconstrained diffusion, the unsaturated probe is certainly not excluded from the region where the domain is located (see the fluorescence within the dashed contour line); it appears slightly enriched in this region compared with the mean intensity. The enrichment varied considerably in consecutive images, allowing only a rough estimation of the partition coefficient as being between 1.6 and 3.0, which is ~50 times weaker partitioning than found for the saturated lipid probe.

Discussion

The current concept of lipid microdomains (Jacobson and Dietrich, 1999) is associated with the co-localization or co-purification of particular components, including GPI-anchored proteins (Sheets *et al.*, 1997; Friedrichson and Kurzchalia, 1998; Simson *et al.*, 1998; Varma and Major, 1998), lipids (Schroeder *et al.*, 1994; Sheets *et al.*, 1997) and transmembrane proteins (Edidin and Stroynowski, 1991; Štefanová *et al.*, 1991; Stauffer and Meyer, 1997). Many of these proteins and lipid components contain saturated acyl chains, suggesting microdomains as more ordered lipid environments (Brown and London, 1998). Modification of the fatty acid composition of the microdomains indeed resulted in significant changes in protein anchorage (Stulnig *et al.*, 1998). Also, lipid association with microdomains appears to be sensitive to the degree of acyl chain saturation since co-purified lipids are predominantly saturated while highly unsaturated lipids are excluded (Schroeder *et al.*, 1994). With regard to the characteristic sizes of microdomains, suggestions range from associations of a few molecules (Friedrichson and Kurzchalia, 1998) up to sizes of several hundred nanometers (Yechiel and Edidin, 1987; Edidin and Stroynowski, 1991; Brown and Rose, 1992; Edidin, 1997; Sheets *et al.*, 1997; Hwang *et al.*, 1998; Simson *et al.*, 1998). Several acronyms are used for such operationally defined microdomains enriched in specialized lipids, including DRMs and DIGs (detergent-insoluble glycolipid-enriched membrane domains), or 'lipid rafts' (Simons and Ikonen, 1997) as perhaps the most descriptive term.

The present study investigated the existence and properties of lipid microdomains as compartments for lipid partitioning within the membrane, by direct imaging of the motion of single lipid probes and of their lateral organization using the SDT method. In view of the common agreement that components with saturated acyl chains are enriched in microdomains, we chose two lipid probes, one with saturated and one with mono-unsaturated acyl chains.

Lipid domains are clearly shown to exist in HASM cell membranes as areas with high local enrichment of the saturated lipid probe. Imaging was performed under the least invasive conditions with 1–20 probes per domain (corresponding to a domain area fraction of 2–40 × 10^{-6} covered by the probe) so that the domain properties, i.e. size, shape and motion, are safely regarded as being unperturbed by the measurement. Domain size was operationally defined (see Results), yielding a broad distribution. This size distribution ranging from 0.2 to 2 μm exactly corresponds to the sizes of DRMs seen in electron micrographs (Brown and Rose, 1992). There was, however, considerable sub-structure in many domains (see also the model for 'macrorafts' in Jacobson and Dietrich, 1999). Repeated imaging of such domains revealed that the apparent shape changes are caused by reorganization of sub-structures rather than by shape fluctuations of one

large structure. Thus, at least parts of the domains were associations of smaller domains, indicating the existence of elementary units of considerably smaller sizes than the mean size of 700 nm. It should be noted that domain properties such as size and number measured here at ambient temperature may well differ at physiological temperature. Preliminary studies of HASM cells at 37°C revealed a reduced domain size, which will be the subject of further analysis.

Perhaps the most interesting finding with respect to the function of the domains is their persistent localization. They were never seen to diffuse freely. When they moved, they did so in a uni-directional fashion. Occasionally, a domain was observed to dissolve or to newly assemble, but at fixed positions. In view of this, we would like to postulate that the lipid microdomains seen are anchored to the membrane skeleton and/or to the cytoskeleton. Similar conclusions were drawn from tracking single proteins via an attached latex sphere (Kusumi and Sako, 1996) and are included in possible raft models (Jacobson and Dietrich, 1999).

Results on kinetics and partitioning of the lipid probes are, in contrast to the results on domain properties, intimately related to the probes used. The distinctly different behavior of the two probes was caused by structurally different acyl chains. The data indicate that the particular polar head of both probes carrying the fluorophore may not significantly perturb the lipid environment since the chains very specifically sense different environments. Therefore, the data for the lipid probes may reflect qualitative features of lipids in the membrane: (i) high partitioning of lipids with saturated chains into domains with relatively fast diffusion; and (ii) much less partitioning of lipids with unsaturated chains predominantly diffusing freely within the bulk membrane.

The observed behavior of the saturated lipid probe in microdomains correlates with lipid properties found in DRMs, which probably originate from lipid rafts (for a discussion, see Jacobson and Dietrich, 1999). In DRMs, containing sphingolipid, cholesterol and saturated phospholipids as the main lipid constituents, lipids with saturated acyl chains show high mobility (Schroeder *et al*., 1994). This appears to be characteristic for membranes containing cholesterol and saturated phospholipids, which assemble to a particular phase, termed the liquid-ordered (l_o) phase (Sankaram and Thompson, 1991; Bloom and Mouritsen, 1995; Ahmed *et al*., 1997). Saturated lipid acyl chains in the liquid-ordered state are tightly packed in all-*trans* configuration with little space for rotational isomerization. Although they are in a low free-energy state, the lipids do not crystallize with cholesterol and show relatively fast lateral diffusion. Reported diffusion constants at room temperature are in agreement with the value found here for lipid probe motion in domains (Almeida *et al*., 1992). The conclusion that domains are highly fluid is in agreement with results of tracking membrane proteins carrying a gold particle (Sheets *et al*., 1997) showing a substantial degree of lateral mobility within confinement domains (Simson *et al*., 1998).

Furthermore, the high partition coefficient of ~100 of the saturated probe into domains indicates a low free-energy state, which is RTln(100) = 11.3 kJ/mol lower than outside domains. An energy of this order appears reasonable for a transition of the chains from a state of extensive isomerization to a tightly packed state (Ipsen *et al*., 1987). Thus, fast diffusion and high partitioning together strongly suggest that the saturated lipid probe in the microdomains is mobile while its chains are more ordered, similarly to properties reported for the l_o-like lipid phase. The coincidence of lipid properties found here in microdomains with those found in DRMs (Schroeder *et al*., 1994), together with the finding of equal size distributions (Brown and Rose, 1992), is taken as strong evidence that we were observing the structural counterpart of DRMs in native membranes of living cells.

The mobility of the unsaturated lipid probe, DOPE-Cy5, within the bulk membrane indicated deviations from free Brownian motion, quantified by a slope parameter $\alpha = 0.87$. Such deviations from $\alpha = 1$ have, so far, been discussed in the literature within the context of anomalous subdiffusion (Saxton, 1994; Feder *et al*., 1996) This model assumes diffusion hindered by unpenetrable, immobile obstacles with a surface density related to α. The value of $\alpha = 0.87$ obtained would indicate within this model a 35% coverage of the HASM cell membrane by obstacles to the diffusion of the unsaturated lipid probe. However, the observation that DOPE-Cy5 shows a slight enrichment in the domains offers an alternative interpretation. Local enrichment is equivalent to increased residence time, thus reducing the long-range mobility of the probe. The extent of reduction depends on the fraction of the probe in domains, which is estimated to be 20–30% from the partition coefficient of 1.6–3 and the 13% area coverage by domains. Assuming that this percentage of the probe molecules stay confined to the domains for the lag times applied, the observed deviation from Brownian motion is accounted for qualitatively. This effect probably adds to the hindrance of diffusion by immobile obstacles, which may be represented by caveolae, occurring at very high density in HASM cell membranes (Thyberg *et al*., 1998) and/or simply by the various membrane proteins and associates with impeded or restricted motion.

In conclusion, the results presented here confirm the current concept of the lateral heterogeneity of plasma membranes in terms of microdomains or lipid rafts, at a quantitative level by describing the properties of lipid microdomains and of lipids therein. It is clear that in approaching microdomains from the perspective of the organization of lipids only, important questions are left unanswered with regard to the function of the observed lipid microdomains and their relationship to lipid rafts or to other compartments such as caveolae. It may be noted, however, that this first report of single molecule imaging by SDT in native cell membranes indicates the feasibility of studies that may address these questions. By imaging not two lipid probes, but the saturated lipid probe and a protein probe simultaneously, one may investigate directly the postulated anchorage of the domains to structural networks, the co-localization of proteins known to be associated with lipid rafts or caveolae, and the function-specific domain properties, opening up a new perspective towards advanced understanding of membrane heterogeneity.

Materials and methods

Syntheses of phospholipid–fluorophore conjugates

Phospholipids were purchased from Sigma, Cy5 from Amersham-Pharmacia-Biotech and TMR from Molecular Probes. For the synthesis

of DMPE-Cy5, 3 mg of DMPE, 7 mg of DOPC and 10 µl of triethylamine were dissolved in 0.5 ml of chloroform, and the contents of one vial of Cy5-monofunctional dye (~100 nmol of active succinimidyl ester) in 0.5 ml of methanol were added. After 30 min of stirring, the dried residue was dissolved in a mixture of chloroform/methanol/water 1/2/1. The organic phase was filtered and dried. The residual solid was dissolved in chloroform/methanol/water 70/30/4, applied to a preparative TLC plate and developed in the same solvent mixture. The product was extracted with chloroform/methanol 2/1. The yield was 15 nmol of DMPE-Cy5 (according to $\varepsilon_{650} = 250\,000$).

DMPE-TMR was synthesized by dissolving 0.5 mg (0.94 µmol) of TMR-NHS ester (TMR-NHS) and 2 mg (3.1 µmol) of DMPE in 1 ml of chloroform/methanol (4/1) containing 10 µl (75 µmol) of triethylamine. After 1 h, the mixture was dried and the crude product was purified by applying it to a reverse phase column (Merck LiChroprep). DMPE-TMR was eluted with 80% organic solvent content (ethanol/*n*-propanol 5/2 was used in place of acetonitrile). The yield was 0.28 mg (260 nmol) of DMPE-TMR (according to $\varepsilon_{550} = 80\,000$).

DOPE-Cy5 was synthesized in the same way as DMPE-Cy5, except that no DOPC was used to dissolve DOPE. The yield was 12 nmol of DOPE-Cy5 (according to $\varepsilon_{650} = 250\,000$).

Cell culture

HSAM cells (Applied Cell Biology Research Institute, Kirkland, WA) were cultured in Dulbecco's modified Eagle's medium without phenol red, supplemented with antibiotics and 10% fetal calf serum, in a humidified atmosphere (95%) at 5% CO_2 and 37°C. Cells were used for 12–14 passages and were transferred every 4 days.

Lipid insertion

For single molecule imaging, lipid vesicles were prepared from a mixture of 1-palmitoyl-2-oleoyl-*sn*-glycero-3-phosphocholine (POPC)/lipid probe (DMPE-Cy5 or DOPE-Cy5) at a molar ratio of 10^3 by sonication for ~30 min. For this, the average diameter of the vesicles is ~20 nm (Huang and Mason, 1978), yielding a fluorophore concentration of 4 ± 2 per vesicle (using an area of 65 Å^2/lipid). Cells were incubated for 15 min with a vesicle solution of 50 µg/ml in phosphate-buffered saline (PBS; 170 mM NaCl, 3 mM KCl, 10 mM Na_2HPO_4, 1.8 mM KH_2PO_4, pH 7.4) at room temperature. Under these conditions, the transfer efficiency of the lipids from vesicles to the cell membrane is low (Malle *et al*., 1994), resulting in a lipid probe concentration of ~1 per 50 µm^2 on the plasma membrane, as determined from SDT images. Subsequently, cells were flushed extensively with PBS to remove vesicles from the measurement chamber. Before fluorescence images were taken, the probes were allowed to equilibrate for at least 10 min within the cell membrane.

For single domain imaging, the same procedures for vesicle preparation and for lipid probe insertion (DMPE-TMR and DOPE-Cy5) were used, except that a higher lipid probe mole fraction in POPC of 10% was applied.

Microscopy

The apparatus, data acquisition and automatic data analysis system were used as described in detail (Schmidt *et al*., 1995). In brief, samples were illuminated by 633 nm light from a dye laser (Model 375B; Spectra Physics, CA) using a 100× objective (PlanNeofluar, NA = 1.3; Zeiss, Oberkochen, Germany) in an epifluorescence microscope (Axiovert 135TV; Zeiss). The laser beam was defocused to an area of 100 µm^2 at a mean intensity of 1.4 kW/cm^2. For all experiments, the illumination time was set to $t_{ill} = 5$ ms. Rayleigh scattered light was blocked effectively by appropriate filter combinations (645 DRLPO2, 670 DF40, Omega, HSPF-632.8-1.0, Kaiser Optical Systems, MI). Images were obtained by a liquid nitrogen-cooled slow-scan CCD camera system (AT200, Photometrix, Tucson, AR, equipped with a TK512CB-chip, Tektronix) and stored on a PC. The delay time (t_{delay}) between two consecutive observations was set to either 7, 25 or 115 ms for DOPE-Cy5 and 10 or 30 ms for DMPE-Cy5. For technical reasons, the number of consecutive images was limited to 14 (Schmidt *et al*., 1995). An automatic analysis program determined the position of each fluorescence labeled molecule, $\vec{r}(t)$, by fitting the single molecule fluorescence image to a two-dimensional Gaussian surface, yielding a positional accuracy of typically 54 nm.

FRAP experiments were performed by taking a sequence of 10 consecutive images with a delay of 13 s. Between the first and the second image, the sample was photobleached. For dual wavelength imaging, the illumination light was switched alternately between 633 nm (dye laser) and 528 nm (2 kW/cm^2, Ar^+ laser, C306; Coherent, Santa Clara, CA) (Schütz *et al*., 1998). The delay between observations at alternative illuminations was set to 25 ms. In experiments at high lipid probe concentration, diffuse background fluorescence due to out-of-focus fluorescence from vesicles adsorbed to the glass slide around the cell was subtracted from all images. Such background fluctuations did not adversely affect analysis of domain properties, but rendered the simultaneous localization of the few single probe molecules in inter-domain areas impossible.

Analysis of single molecule trajectories

Single molecule trajectories were analyzed according to previous studies (Bobroff, 1986; Kusumi *et al*., 1993; Schütz *et al*., 1997). The mean square displacement, $\langle r^2(t_{lag})\rangle = \langle(\vec{r}(t + t_{lag}) - \vec{r}(t))^2\rangle$, was calculated for all time lags $t_{lag} = t_{ill} + t_{delay}$. For determination of corralled diffusion, data were fitted according to the exact solution for restricted diffusion within a square of side length L and with a free diffusion constant D:

$$\langle r^2\rangle(t) = \frac{L^2}{3} - \frac{8L^2}{\pi^4} \sum_{n\,=\,1(odd)}^{\infty} \frac{1}{n^4} \exp\left\{-\frac{n^2\pi^2 D}{L^2}\,t\right\}$$

(Kusumi *et al*., 1993).

Acknowledgements

We would like to thank Thomas Schmidt for critical discussions on diffusion models, Hermann J.Gruber for instructions on lipid labeling, Klaus Groschner for providing the HASM cell line, and Heike Kahr for keeping our cells alive. We are also grateful to Ken Jacobson for critical and encouraging comments on the manuscript. This work was supported by the Austrian Ministry of Science, projects GZ 200.027/2 and GZ 200.027/3, by the Austrian Research Funds, P12803-MED and the EC-BIOTECHNOLOGY program project ERBBIO4CT960592.

References

Ahmed,S.N., Brown,D.A. and London,E. (1997) On the origin of sphingolipid/cholesterol rich detergent-insoluble cell membranes: physiological concentrations of cholesterol and sphingolipid induce formation of a detergent-insoluble, liquid-ordered lipid phase in model membranes. *Biochemistry*, **36**, 10944–10953.

Almeida,P.F.F., Vaz,W.L.C. and Thompson,T.E. (1992) Lateral diffusion in the liquid phases of dimyristoylphosphatidylcholine/cholesterol lipid bilayers: a free volume analysis. *Biochemistry*, **31**, 6739–6747.

Anderson,R.G. (1998) The caveolae membrane system. *Annu. Rev. Biochem.*, **67**, 199–225.

Anderson,R.G., Kamen,B.A., Rothenberg,K.G. and Lacey,S.W. (1992) Potocytosis: sequestration and transport of small molecules by caveolae. *Science*, **255**, 410–411.

Atkins,P.W. (1978) *Physical Chemistry.* Oxford University Press, Oxford, UK.

Bobroff,N. (1986) Position measurement with a resolution and noise-limited instrument. *Rev. Sci. Instrum.*, **57**, 1152–1157.

Bloom,M. and Mouritsen,O.G. (1995) The evolution of membranes. In Lipowsky,R. and Sackmann,E. (eds), *Handbook of Biological Physics*. Elsevier/North Holland, Amsterdam, The Netherlands, Vol. 1, pp. 65–95.

Brown,D.A. and London,E. (1998) Structure and origin of ordered lipid domains in biological membranes. *J. Membr. Biol.*, **164**, 103–114.

Brown,D.A. and Rose,J.K. (1992) Sorting of GPI-anchored proteins to glycolipid-enriched membrane subdomains during transport to the apical cell surface. *Cell*, **68**, 533–544.

Chang,W.-J. *et al*. (1994) Purification and characterization of smooth muscle cell caveolae. *J. Cell Biol.*, **126**, 127–138.

Edidin,M. (1997) Lipid microdomains in cell surface membranes. *Curr. Opin. Struct. Biol.*, **7**, 528–532.

Edidin,M. and Stroynowski,I. (1991) Differences between the lateral organization of conventional and inositol phospholipid-anchored membrane proteins. A further definition of micrometer scale membrane domains. *J. Cell Biol.*, **112**, 1143–1150.

Enderle,Th., Ogletree,D.F., Chemla,D.S., Magowan,C. and Weiss,S. (1997) Membrane specific mapping and colocalization of malarial and host skeletal proteins in the *Plasmodium falciparum* infected erythrocyte by dual-color near-field scanning optical microscopy. *Proc. Natl Acad. Sci. USA*, **94**, 520–525.

Feder,T.J., Brust-Mascher,I., Slattery,J.P., Baird,B. and Webb,W.W.

(1996) Constrained diffusion or immobile fraction on cell surfaces: a new interpretation. *Biophys. J.*, **70**, 2767–2773.
Fielding,P.E. and Fielding,C.J. (1995) Plasma membrane caveolae mediate the efflux of cellular free cholesterol. *Biochemistry*, **34**, 14288–14292.
Friedrichson,T. and Kurzchalia,T.V. (1998) Microdomains of GPI-anchored proteins in living cells revealed by crosslinking. *Nature*, **394**, 802–805.
Funatsu,T., Harada,Y., Tokunaga,M., Saito,K. and Yanagida,T. (1995) Imaging of single fluorescent molecules and individual ATP turnovers by single myosin molecules in aqueous solution. *Nature*, **374**, 555–559.
Harder,T. and Simons,K. (1997) Caveolae, DIGs, and the dynamics of sphingolipid–cholesterol microdomains. *Curr. Opin. Cell Biol.*, **9**, 534–542.
Hinterdorfer,P., Gruber,H.J., Striessnig,J., Glossman,H. and Schindler,H. (1997) Analysis of membrane protein self-association in lipid systems by fluorescence particle counting: application to the dihydropyridine receptor. *Biochemistry*, **36**, 4497–4504.
Huang,C. and Mason,J.T. (1978) Geometric packing constraints in egg phosphatidylcholine vesicles. *Proc. Natl Acad. Sci. USA*, **75**, 308–310.
Hwang,J., Gheber,L.A., Margolis,L. and Edidin,M. (1998) Domains in cell plasma membranes investigated by near-field scanning optical microscopy. *Biophys. J.*, **74**, 2184–2190.
Ishijima,A., Kojima,H., Funatsu,T., Tokunaga,M., Higuchi,H., Tanaka,H. and Yanagida,T. (1998) Simultaneous observation of individual ATPase and mechanical events by a single myosin molecule during interaction with actin. *Cell*, **92**, 161–171.
Ipsen,J.H., Karlström,G., Mouritsen,O.G., Wennerström,H. and Zuckermann,M.J. (1987) Phase equilibria in the phosphatidylcholine–cholesterol system. *Biochim. Biophys. Acta*, **905**, 162–172.
Jacobson,K. and Dietrich,C. (1999) Looking at lipid rafts? *Trends Cell Biol.*, **9**, 87–91.
Kusumi,A. and Sako,Y. (1996) Cell surface organization by the membrane skeleton. *Curr. Opin. Cell Biol.*, **8**, 566–574.
Kusumi,A., Sako,Y. and Yamamoto,M. (1993) Confined lateral diffusion of membrane receptors as studied by single particle tracking (Nanovid microscopy). Effects of calcium-induced differentiation in cultured epithelial cells. *Biophys. J.*, **65**, 2021–2040.
Lu,H.P., Xun,L. and Xie,X.S. (1998) Single-molecule enzymatic dynamics. *Science*, **282**, 1877–1882.
Malle,E., Schwengerer,E., Paltauf,F. and Hermetter,A. (1994) Transfer of pyrene-labelled diacyl-, acylacyl-, and alkenylacyl-glycero-phospholipids from vesicles to human blood platelets. *Biochim. Biophys. Acta*, **1189**, 61–64.
Melkonian,K.A., Chu,T., Tortorella,L.B. and Brown,D.A. (1995) Characterization of proteins in detergent-resistant membrane complexes from Madin-Darby canine kidney epithelial cells. *Biochemistry*, **34**, 16161–16170.
Parton,R.G. (1996) Caveolae and caveolins. *Curr. Opin. Cell Biol.*, **8**, 542–548
Sankaram,M.B. and Thompson,T.E. (1991) Cholesterol-induced fluid-phase immiscibility in membranes. *Proc. Natl Acad. Sci. USA*, **88**, 8686–8690.
Sargiacomo,M., Sudol,M., Tang,Z.L. and Lisanti,M.P. (1993) Signal transducing molecules and glycosyl-phosphatidylinositol-linked proteins form a caveolin-rich insoluble complex in MDCK cells. *J. Cell Biol.*, **122**, 789–807.
Sase,I., Miyata,H., Corrie,J.E.T., Craik,J.S. and Kinosita,K.,Jr (1995) Real time imaging of single fluorophores on moving actin with an epifluorescence microscope. *Biophys. J.*, **69**, 323–328.
Saxton,M. (1994) Anomalous diffusion due to obstacles: a Monte Carlo study. *Biophys. J.*, **66**, 394–401.
Schmidt,Th., Schütz,G.J., Baumgartner,W., Gruber,H.J. and Schindler,H. (1995) Characterization of photophysics and mobility of single molecules in a fluid lipid membrane. *J. Phys. Chem.*, **99**, 17662–17668.
Schmidt,Th., Schütz,G.J., Baumgartner,W., Gruber,H.J. and Schindler,H. (1996) Imaging of single molecule diffusion. *Proc. Natl Acad. Sci. USA*, **93**, 2926–2929.
Schmidt,Th., Hinterdorfer,P. and Schindler,H. (1999) Microscopy for recognition of individual biomolecules. *Microsc. Res. Tech.*, **44**, 339–346.
Schnitzer,J.E., McIntosh,D.P., Dvorak,A.M., Liu,J. and Oh,P. (1995) Separation of caveolae from associated microdomains of GPI-anchored proteins. *Science*, **269**, 1435–1439.
Schroeder,R., London,E. and Brown,D. (1994) Interactions between saturated acyl chains confer detergent resistance on lipids and glycosylphosphatidylinositol (GPI)-anchored proteins: GPI-anchored proteins in liposomes and cells show similar behavior. *Proc. Natl Acad. Sci. USA*, **91**, 12130–12134.
Schütz,G.J., Schindler,H. and Schmidt,Th. (1997) Single-molecule microscopy on model membranes reveals anomalous diffusion. *Biophys. J.*, **73**, 1073–1080.
Schütz,G.J., Trabesinger,W. and Schmidt,Th. (1998) Direct observation of ligand colocalization on individual receptor molecules. *Biophys. J.*, **74**, 2223–2226.
Sheets,E.D., Lee,G.M., Simson,R. and Jacobson,K. (1997) Transient confinement of a glycosylphosphatidylinositol-anchored protein in the plasma membrane. *Biochemistry*, **36**, 12449–12458.
Simons,K. and Ikonen,E. (1997) Functional rafts in cell membranes. *Nature*, **387**, 569–572.
Simson,R., Yang,B., Moore,S.E., Doherty,P., Walsh,F.S. and Jacobson,K.A. (1998) Structural mosaicism on the submicron scale in the plasma membrane. *Biophys. J.*, **74**, 297–308.
Stauffer,Th. and Meyer,T. (1997) Compartmentalized IgE receptor-mediated signal transduction in living cells. *J. Cell Biol.*, **139**, 1447–1454.
Štefanová,I., Hořejši,V., Ansotegui,I.J., Knapp,W. and Stockinger,H.. (1991) GPI-anchored cell-surface molecules complexed to tyrosine kinases. *Science*, **254**, 1016–1019.
Stulnig,Th.M., Berger,M., Sigmund,Th., Raederstorff,D., Stockinger,H. and Waldhäusl,W. (1998) Polyunsaturated fatty acids inhibit T cell signal transduction by modification of detergent-insoluble membrane domains. *J. Cell Biol.*, **143**, 637–644.
Szabo,A., Schulten,K. and Schulten,Z. (1980) First passage time approach to diffusion controlled reactions. *J. Chem. Phys.*, **72**, 4350–4357.
Thyberg,J., Roy,J., Tran,P.K., Blomgren,K., Dumitrescu,A. and Hedin,U. (1997) Expression of caveolae on the surface of rat arterial smooth muscle cells is dependent on the phenotypic state of the cells. *Lab. Invest.*, **77**, 93–101.
Trabesinger,W. (1997) Single molecule microscopy in biosystems. Photobleaching and colocalization studies. Diploma thesis, University of Linz, Linz, Austria.
Varma,R. and Mayor,S. (1998) GPI-anchored proteins are organized in submicron domains at the cell surface. *Nature*, **394**, 798–801.
Weiss,S. (1999) Fluorescence spectroscopy of single biomolecules. *Science*, **283**, 1676–1683.
Yechiel,Y. and Edidin,M. (1987) Micrometer-scale domains in fibroblast plasma membranes. *J. Cell Biol.*, **105**, 755–760.

Received November 8, 1999; revised and accepted January 12, 2000